

NeurSF: Neural Shading Field for Image Harmonization

Zhongyun Hu* Ntumba Elie Nsampi* Xue Wang Qing Wang
Northwestern Polytechnical University

Abstract

Image harmonization aims at adjusting the appearance of the foreground to make it more compatible with the background. Due to a lack of understanding of the background illumination direction, existing works are incapable of generating a realistic foreground shading. In this paper, we decompose the image harmonization into two sub-problems: 1) illumination estimation of background images and 2) rendering of foreground objects. Before solving these two sub-problems, we first learn a direction-aware illumination descriptor via a neural rendering framework, of which the key is a Shading Module that decomposes the shading field into multiple shading components given depth information. Then we design a Background Illumination Estimation Module to extract the direction-aware illumination descriptor from the background. Finally, the illumination descriptor is used in conjunction with the neural rendering framework to generate the harmonized foreground image containing a novel harmonized shading. Moreover, we construct a photo-realistic synthetic image harmonization dataset that contains numerous shading variations by image-based lighting. Extensive experiments on this dataset demonstrate the effectiveness of the proposed method. Our dataset and code will be made publicly available.

1. Introduction

Given a composite image of which the foreground and background taken from different images, image harmonization aims to adjust the appearance of the foreground to make it compatible with the background. A lot of works [8, 10, 16, 21, 22, 36, 41, 47] have been proposed to solve the inharmony problem in composite images. These image harmonization methods, however, tend to focus on adjusting the low-level statistics (i.e., color and brightness) of the foreground region rather than its shading.

The failure to model shading of existing methods can be attributed to their lack of a comprehensive understanding of the background illumination, since they cannot perceive the directional information of illumination. Learning-based

methods, such as [10, 16, 22, 36], are generally formulated as the image-to-image translation task where the illumination is implicitly transferred from the background region to the foreground object. Moreover, existing large-scale image harmonization datasets [10, 36] are devoid of perceivable shading variations. Therefore, it is unclear whether the methods based on these datasets can effectively deal with shading variations.

To avoid the intensive labor associated with the collection and construction of large real-world harmonization datasets, existing works have turned to synthetic data [10]. Color transfer algorithms [15, 27, 29, 39] have been used to generate visually acceptable images with varying color and brightness. However, the shading variation, which is also an important component during image harmonization, is not taken into consideration. To this end, we construct the first large-scale photo-realistic image harmonization dataset that contains color, brightness and shading variations through image-based lighting [12]. In addition, unlike synthetic datasets [8] of which the foreground objects and illumination maps are both created by CG software, we refer to real models/illumination captured from the real world, with the aim of achieving photo-realistic renderings.

In this paper, we propose to decompose the image harmonization task into two sub-problems: (1) illumination estimation of background images, and (2) rendering of foreground objects under background illuminations. The general lighting representation (i.e. illumination maps [14]) that is able to record the complete illumination can be used to solve sub-problem (1), however, using such a representation brings considerable challenges due to its large number of parameters. Our key to solving (1) lies in the proposal of an efficient illumination representation that can well retain directional information and meanwhile has fewer parameters. For sub-problem (2), in contrast to the spherical harmonics lighting model [28], we intend to render complex visual effects such as cast shadows to further improve the realism of composite images. We propose a novel neural rendering framework that accounts for cast shadows while learning a direction-aware illumination descriptor from the illumination maps. Once we pre-define the direction-aware illumination descriptor, the descriptor of the background

*Authors contributed equally to this work.

image is first extracted using the Background Illumination Estimation Module and then is used in conjunction with our neural rendering framework to generate the harmonized foreground image which contains a harmonized shading.

Different from previous image harmonization methods [10, 16, 22, 36], we also consider the image harmonization problem in view of the recent commoditization of cameras that simultaneously provide color and depth images. We only capture the depth information of foreground objects and omit the background. This is mainly because the objects of interest are usually considered as a foreground class in real life and their 3D models can be acquired easily by the devices, while the background stays far away and is usually collected for image composition. By leveraging depth information, we propose a neural shading model to decompose the shading field into multiple shading components, which are then combined with the illumination descriptor to render the foreground shading.

Our contributions can be summarized as follows:

1. We release the first photo-realistic synthesized image harmonization dataset that contains shading variations.
2. We design a novel neural rendering framework to learn a direction-aware illumination descriptor from the illumination maps in a self-supervised manner.
3. We propose a neural Shading Module that decomposes the shading field into multiple shading components to generate the foreground shading using the direction-aware illumination descriptor estimated from the background. To the best of our knowledge, this is the first to explicitly model shading in image harmonization.

2. Related Work

In this section, we briefly discuss existing works related to image harmonization. In addition, image relighting methods relevant to the proposed work are also included.

2.1. Image Harmonization

Traditional image harmonization methods [6, 18, 21, 25–27, 29, 35, 41] focus on matching low-level statistics between images. The pioneer work [29] matched the means and variances of the color histograms between images in a decorrelated color space. Lalonde and Efros [21] then combined global color statistics obtained over a large natural image set and local color statistics to improve the realism of the composite images. Sunkavalli et al. [35] proposed to match contrast, texture, noise, and blur of visual appearance using multi-scale pyramid representations to produce realistic composites. Xue et al. [41] identified key statistical measures that most affect the realism of a composite

image. However, the adjustment of low-level statistics can not handle shading variations.

In the past few years, researchers have concentrated on deep neural network-based approaches for image harmonization [8, 10, 11, 16, 17, 22, 32, 33, 36, 47]. Zhu et al. [47] proposed a CNN-based classifier model for the perception of realism to guide a traditional color adjustment method to produce more realistic outputs. The first end-to-end CNN model for image harmonization was proposed by Tsai et al. [36]. Existing deep neural network-based image harmonization approaches usually formulate image harmonization as an image-to-image translation problem, and consider ensuring the visual consistency between the foreground and the background in different aspects, such as the domain consistency [9, 10], the visual style consistency [22], and the reflectance/illumination consistency [16]. In [11] and [17], the attention mechanism is applied to consider feature differences between the foreground and background, which leads to better results. However, from the perspective of physical image formation, learning-based image harmonization methods lack the perception of illumination information in the background image, especially the direction of illumination. This inevitably leads to their inability to generate a realistic foreground shading, which severely degrades the realism of composite images. In contrast, we propose to extract a direction-aware descriptor from the background image, and then apply it in a neural rendering framework to generate a new foreground shading that conforms to the background illumination.

2.2. Image Relighting

Traditional image-based relighting methods [13, 23, 40] directly reconstruct the light transport function to relight the objects using multiple images under different illumination conditions. Note that the illumination here is always explicitly provided. Recently, several deep neural networks with illumination estimation modules [19, 20, 31, 34, 38, 46] are proposed to relight objects of a specific class (e.g., portraits and human bodies) using a single RGB image. Still, the illumination estimation is only considered for specific objects rather than natural scenes. Given multi-view images, Yu et al. [42] proposed the first single image-based outdoor scene relighting method along with lighting estimation for the scene. They used the spherical harmonics lighting [28] to generate the shading and it could not handle cast shadows caused by occlusion. Moreover, it is worth noting that although these relighting methods [19, 20, 31, 34, 38, 42, 46] with illumination estimation can be applied to image harmonization, additional computational overhead would be introduced, since illumination estimation for the background image is often accompanied by the estimation of other physical attributes in the background image. In other words, these relighting methods are not

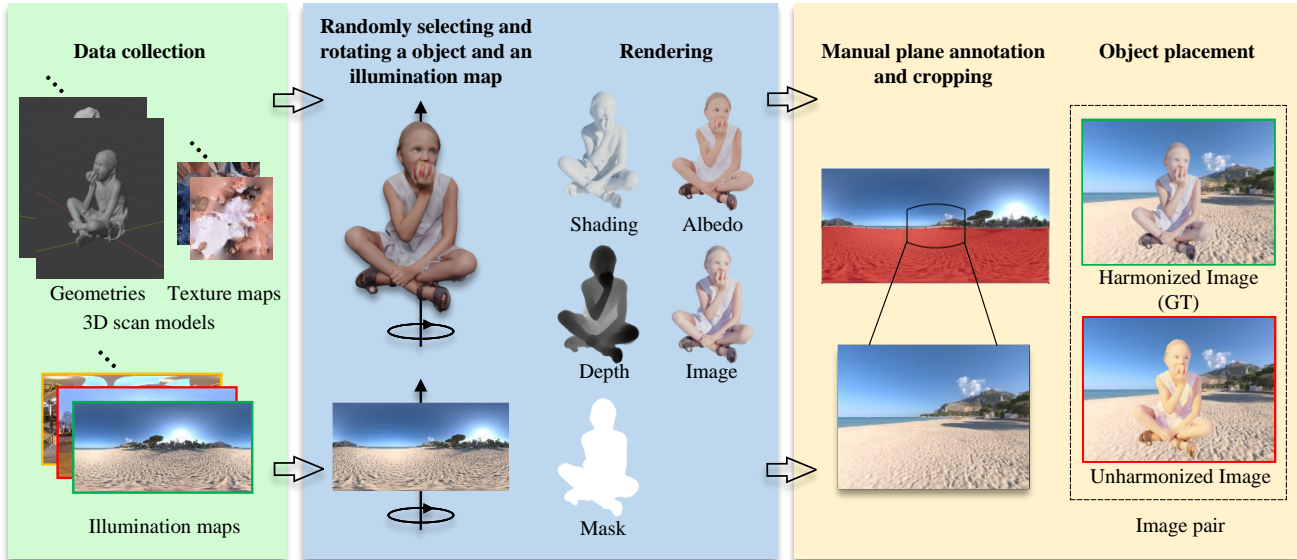


Figure 1. The pipeline of constructing the pair of harmonized image and unharmonized image.

specifically designed for image harmonization. Differently, we consider the problem of image harmonization using a single RGB-D image, hence how to utilize the depth information is the key to our method.

3. Image Harmonization Dataset

The goal of our image harmonization dataset is to introduce a new challenging benchmark with photo-realistic synthesized images and plentiful variations (color, brightness, and shading) to the community of image harmonization. The pipeline of constructing the pair of harmonized image (ground truth) and unharmonized image is illustrated in Fig. 1. Below we introduce the construction process, which covers both data collection, rendering and object placement.

3.1. Data Collection

To construct our dataset, we collect both high-quality 3D human models and high dynamic range (HDR) illumination maps. The collected 3D models are acquired from [1] using photogrammetric 3D scanning methods. A rich variety of humans are included, with the diversity across genders (male, female), ages, poses, and clothing (colors, accessories). We collect a total of 139 high-quality 3D humans, of which 120 are used for training and 19 for testing.

Our illumination maps are collected from the internet source Poly Haven [3] and HDR MAPS [2], which offers diverse high dynamic range panoramic images. We mainly select outdoor illumination maps and omit indoor ones, resulting in a total of 360 high dynamic range panoramic images. We ensure that the selected illumination maps are diverse across weather conditions (sunny, cloudy, and

overcast), illuminant colors, time of the day, and locations. From the 360 images, 222 images are used for training and the remaining 138 ones are reserved for testing. All the selected illumination maps come with the resolution of 8k, which are resized to 2k before rendering.

3.2. Rendering

To generate the training and test images, we use blender [7] with the Cycle Renderer. Each object is first placed on a planar surface within the blender environment. We then randomly sample (without replacement) half of the total number of images as illumination maps. For each possible pair of object and illumination map, we randomly sample 4 rotation angles from a pre-defined range of 8 angles, ranging from 0 to 360 degrees with an increment of 45 degrees. The sampled angles are used to rotate both the object and the illumination map, resulting in a total of 16 path-traced images per object. This increases the richness of object poses and provides sufficient shading variations for our model to learn.

For each object, we generate path-traced images, shading images, albedo images, depth maps, and foreground masks, which are all rendered with a resolution of 480 x 640 pixels. About 100~200 samples per pixel are used for generating path-traced images.

3.3. Object Placement

The location of an object within an image can convey important clues for image harmonization algorithms. Here, object placement and the tuple building for training and test sets will be elaborated. We assume that all objects within

Scene	Sunny	Sunrise/Sunset	Cloudy	Night	All
#Train	88,320	40,320	67,200	17,280	213,120
#Test	14,896	4,320	8,912	656	28,784

Table 1. The numbers of training and test images on each scene.

an image are placed on planar surfaces. To differentiate between planar and non-planar surfaces within an image, we manually annotate planar surfaces in the illumination maps from which background images will be extracted.

For a given image crop extracted from an illumination map using a virtual camera, we randomly select a pixel from the annotated planar surface. Note that we discard the image crop that does not have the annotated plane surface. We then crop the rendered object from its own image (foreground image), and select one image corner as the reference point. Finally, we randomly resize the cropped object and composite it with the background image, such that the reference point lands on the randomly selected pixel.

To create training and test tuples, we first select a rendered image of an object and its corresponding illumination map. We then rotate the illumination map based on the angle used for rendering and extract an image crop (background image) using a virtual camera. Lastly, we perform the object placement and compose the foreground and background images as described above. The same procedure is used to create both unharmonized and harmonized images, only the unharmonized image contains the same object rendered under a different illumination.

3.4. Dataset Summary

Our dataset has a total of 213,120 training images, and 28,784 test images. We further split the training and the test set based on illumination conditions as reported in Tab. 1. Each image for both the training and the test set comes with an object foreground binary mask. Our images cover a wide range of scenes and illumination conditions.

4. Method

We decompose the image harmonization task into two sub-problems: (1) illumination estimation of background images, and (2) rendering of foreground objects. The overall pipeline of the proposed image harmonization algorithm is shown in Fig. 2. We first train a neural rendering framework to learn the direction-aware illumination descriptor in a self-supervised manner (Sec. 4.1). Then we train a Background Illumination Estimation Module to estimate the direction-aware illumination descriptor from the background image (Sec. 4.3). Finally, the training and implementation details are elaborated in Sec. 4.4.

4.1. Neural Rendering Framework

As shown in Fig. 2(a), the neural rendering framework is composed of three neural network modules and one rendering module. First, the Shading Module and the Illumination Encoder Module generate the shading using the input depth and illumination map. Then, the Albedo Estimation Module makes an estimate of the albedo from the input image. Finally, the Rendering Module uses the albedo feature, shading, and the input image to re-render the input image under novel illumination. Below we describe these four modules in detail.

Shading Module. Inspired by the illumination cone theory [5], the Shading Module f , parameterized by θ_f , is designed to generate a set of shading bases $SB \in \mathbb{R}^{K \times H \times W}$, given the input depth $D \in \mathbb{R}^{H \times W}$ and its surface normal $N \in \mathbb{R}^{3 \times H \times W}$,

$$SB = f(D, N; \theta_f). \quad (1)$$

Here the surface normal is estimated from the input depth and its camera intrinsic parameters using the plane fitting method [24]. The Shading Module, based on a U-Net architecture [30], consists of a downsampling sub-module and an upsampling sub-module. The downsampling sub-module is mainly composed of a series of Residual Dense Blocks [44] (RDBs) followed by max-pooling layers. The upsampling sub-module is composed of several convolution layers and upsampling layers. In addition, we utilize the Global Attention Block (GAB) at the bottleneck of the downsampling sub-module to account for long-range interactions between distant pixels. The GAB is implemented by 6 transformer layers [36]. This enables our network to generate cast shadows caused by occlusions.

Illumination Encoder Module. The purpose of the Illumination Encoder Module g is to encode the illumination map $L \in \mathbb{R}^{3 \times H' \times W'}$ as a low dimensional illumination descriptor $l \in \mathbb{R}^{3 \times K}$,

$$l = g(L; \theta_g), \quad (2)$$

where $K \ll H' \times W'$. In addition, in order to be direction-aware and shadow rendering-aware, our illumination descriptor combines shading bases to generate the final shading $\hat{S} \in \mathbb{R}^{3 \times H \times W}$ that contains all lighting effects,

$$\hat{S}_{cij} = \sum_{k=1}^K l_{ck} \times SB_{kij}. \quad (3)$$

The network architecture of the Illumination Encoder Module is similar to the downsampling sub-module of the Shading Module. The only difference is that the transformer layers are removed to reduce the network parameters and three fully-connected layers are added to output the illumination descriptor. Each fully-connected layer is followed

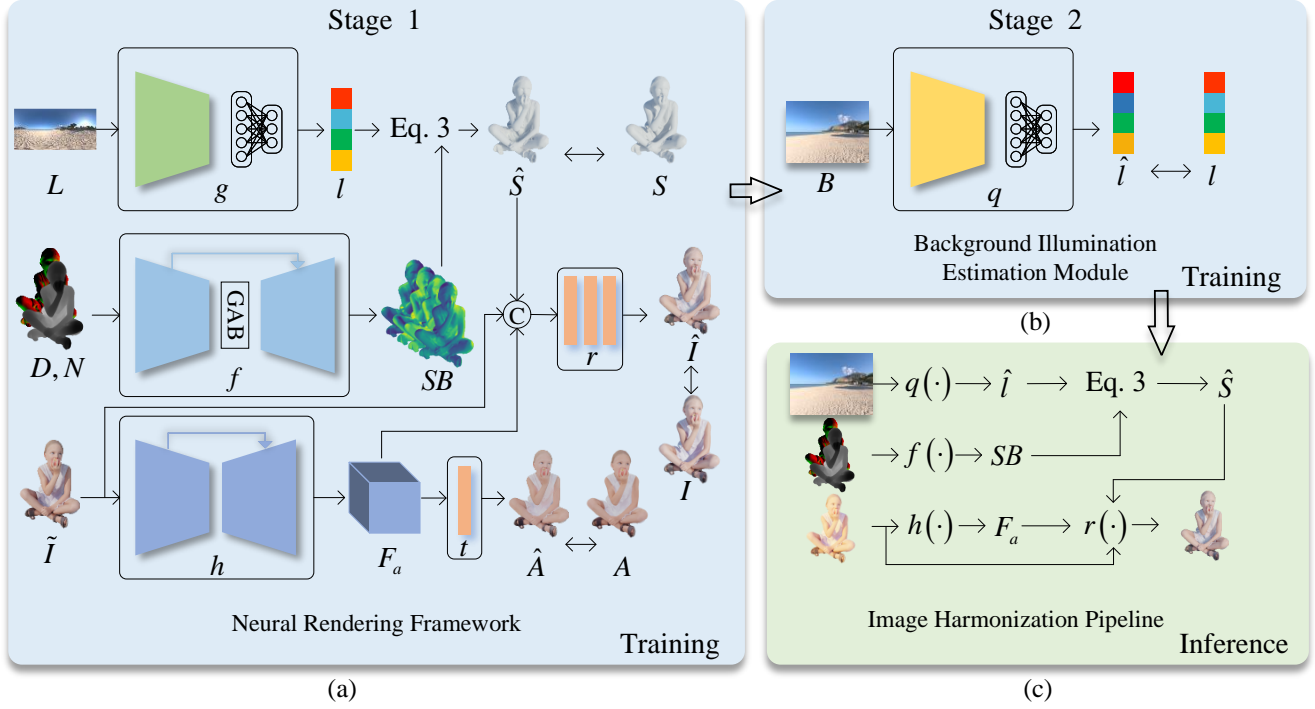


Figure 2. An overview of our proposed image harmonization algorithm.

by a rectified linear activation function except the last fully-connected layer.

Albedo Estimation Module. The Albedo Estimation Module h is designed to extract the albedo feature $F_a \in \mathbb{R}^{C \times H \times W}$ from the input unharmonized image $\tilde{I} \in \mathbb{R}^{3 \times H \times W}$,

$$F_a = h(\tilde{I}; \theta_h). \quad (4)$$

Then, one convolution layer t that takes F_a as input is used to estimate the albedo $\hat{A} \in \mathbb{R}^{3 \times H \times W}$: $\hat{A} = t(F_a; \theta_t)$.

The network architecture of the Albedo Estimation Module is the same as that of the Shading Module without the GAB. In addition, the channel number of RDBs is also reduced by half.

Rendering Module. When both albedo feature and shading are obtained, the Rendering Module r performs the final rendering,

$$\hat{I} = r(F_a, \hat{S}, \tilde{I}; \theta_r). \quad (5)$$

Note that the output image \hat{I} has the same content as the input image \tilde{I} but under another illumination condition L .

The Rendering Module consists of 6 convolution layers and each is followed by a rectified linear activation function.

4.2. Background Illumination Estimation

Once we have obtained the direction-aware illumination descriptor in the neural rendering framework, the goal of

the Background Illumination Estimation Module q , which is shown in Fig. 2 (b), is to estimate the illumination descriptor given the input background image $B \in \mathbb{R}^{3 \times H \times W}$,

$$\hat{l} = q(B; \theta_q). \quad (6)$$

The network architecture of the Background Illumination Estimation Module is the same as that of the Illumination Encoder Module.

4.3. Image Harmonization Pipeline

As shown in Fig. 2(c), our image harmonization pipeline consists of two modules, namely Background Illumination Estimation Module q and Foreground Rendering Module $\{f, h, r\}$.

The Foreground Rendering Module leverages partial modules of the existing neural rendering framework to re-render the input unharmonized foreground image to make it more compatible with the background image.

4.4. Training and Implementation Details

We train the model on our image harmonization dataset with ground truth $\{I, A, S, L\}$, where I, A, S denote harmonized image, albedo and shading respectively. Our training has two stages: training the Neural Rendering Framework and training the Background Illumination Estimation Module.

Sub-dataset	Evaluation Metric	Input Composite	Lalonde and Efron [21]	DoveNet [10]	DoveNet w/ D, N	Guo et al. [16]	Guo et al. w/ D, N	RainNet [22]	RainNet w/ D, N	Ours
Sunny	fMAE↓	0.103	0.146	0.081	0.074	0.077	0.075	0.078	0.073	0.071
	fPSNR↑	19.12	16.26	20.85	21.78	21.09	21.45	21.18	21.72	21.87
	fSSIM↑	0.813	0.773	0.854	0.877	0.848	0.870	0.854	0.877	0.878
	LPIPS↓	0.017	0.040	0.014	0.013	0.015	0.015	0.013	0.013	0.012
Sunrise/Sunset	fMAE↓	0.086	0.138	0.063	0.060	0.067	0.066	0.064	0.064	0.059
	fPSNR↑	21.01	16.82	23.29	23.76	22.49	22.82	23.14	23.19	23.52
	fSSIM↑	0.876	0.823	0.911	0.919	0.901	0.910	0.910	0.914	0.918
	LPIPS↓	0.016	0.038	0.011	0.011	0.013	0.013	0.011	0.012	0.010
Cloudy	fMAE↓	0.084	0.144	0.068	0.063	0.067	0.066	0.066	0.063	0.057
	fPSNR↑	21.55	16.68	23.03	23.82	22.93	23.23	23.37	23.51	24.09
	fSSIM↑	0.888	0.826	0.915	0.924	0.909	0.916	0.919	0.922	0.930
	LPIPS↓	0.014	0.039	0.011	0.010	0.012	0.012	0.010	0.011	0.009
Night	fMAE↓	0.162	0.134	0.094	0.101	0.095	0.099	0.104	0.107	0.105
	fPSNR↑	15.86	17.40	20.63	19.93	20.27	20.24	19.79	19.11	19.34
	fSSIM↑	0.762	0.778	0.853	0.844	0.840	0.840	0.843	0.833	0.843
	LPIPS↓	0.031	0.036	0.018	0.019	0.020	0.020	0.018	0.021	0.020
All	fMAE↓	0.096	0.144	0.075	0.069	0.073	0.071	0.073	0.070	0.066
	fPSNR↑	20.08	16.50	21.89	22.67	21.85	22.18	22.12	22.43	22.75
	fSSIM↑	0.845	0.797	0.881	0.897	0.874	0.889	0.882	0.896	0.899
	LPIPS↓	0.016	0.039	0.013	0.012	0.014	0.014	0.012	0.012	0.011
	Parameters↓	-	-	54.756M	54.756M	40.863M	40.863M	54.763M	54.763M	8.120M

Table 2. Quantitative evaluation on our test set. The best results are highlighted in green. The second best results are highlighted in yellow.

At the first stage, we train the Neural Rendering Framework. We use the \mathcal{L}_1 loss for both shading, albedo and the output image. In addition, inspired by [45], the SSIM metric is utilized to make the neural network learn to produce visually pleasing images. Thus, the loss L_{NR} for the Neural Rendering Framework is defined as,

$$L_{NR} = \|S - \hat{S}\|_1 + \|A - \hat{A}\|_1 + \|I - \hat{I}\|_1 + \lambda(1 - \text{SSIM}(S, \hat{S})) + \lambda(1 - \text{SSIM}(A, \hat{A})) + \lambda(1 - \text{SSIM}(I, \hat{I})), \quad (7)$$

where λ is set to 1 in our experiments.

At the second stage, we train the Background Illumination Estimation Module. The \mathcal{L}_1 loss is used for the illumination descriptor. Also, the predicted illumination descriptor and the shading bases are utilized to render the shading and then minimize the error between the rendered shading and the ground truth shading. The loss L_{BIE} for the Background Illumination Estimation Module is defined as,

$$L_{BIE} = \|g(L) - \hat{l}\|_1 + \left\| S - \sum_k \hat{l}_{ck} \times BS_{kij} \right\|_1. \quad (8)$$

5. Experiments

In this section, to validate the effectiveness of our image harmonization pipeline, we first compare our method with state-of-the-art methods both qualitatively and quantitatively. Then we compare our neural illumination descriptor against the common illumination representation (i.e., HDR illumination maps) to demonstrate its advantages in

terms of rendering quality. Finally, we perform extensive ablation studies to illustrate the contribution of each component of our framework in isolation.

5.1. Experimental Setup

Evaluation metrics. We evaluate the realism of harmonized images using fMAE, fPSNR, fSSIM [37] and LPIPS [43], where f denotes the metric measurements are calculated only using the foreground region.

Baselines. We compare with both traditional method [21] and deep learning-based methods [10, 16, 22]. For deep learning-based methods, we select recent open-source methods achieving state-of-the-art performance. For a fair comparison, we train their models on our image harmonization dataset according to the experiment settings given by the authors. We report their results when the training losses converge.

5.2. Comparison with state-of-the-art

Quantitative results. Tab. 2 summarizes the quantitative results obtained by our method as well as those obtained by competing methods. Our method achieves the best results on the *cloudy* and *sunny* scenes, which can be attributed to its ability to generate realistic shadings. However, our method achieves lower scores on the *night* scene compared to previous works. This is primarily due to the night images lacking noticeable shading variations. Overall, our method achieves the best scores on all metrics when evaluated on the entire test set.

We demonstrate the effects of using depth and normal



Figure 3. Qualitative comparison of different methods on our test set.

information by training the baselines with depth and normal images as additional inputs. As can be observed from Tab. 2, using depth and normals as additional inputs leads to an increase in the rendering performance.

We also compare our method against the baselines in terms of model parameter count. Despite its complexity, our entire framework has a total of 8.1 million parameters, which is approximately one-fifth of the parameter count of the second-best baseline with 40.8 million parameters.

Qualitative results. Harmonized images produced by different methods are shown in Fig. 3. We display qualitative results for several scenes with different lighting conditions, which include *sunny*, *cloudy*, *sunrise/sunset*, and *night* scenes. Our method produces compelling results that are closer to the ground truth in terms of photo-realism. For

instance, in the first column of Fig. 3, there is an observable illumination inconsistency between the foreground and the background of the input image. Specifically, the background suggests that the main illumination source is located at the right front, whereas, the foreground appears to be illuminated from the back. The result of Lalonde et al. [21] shows greenish colors, and all the other comparative methods [10, 16, 22] retain original illumination. In contrast, our method consistently relights the foreground object, making it more consistent with the background illumination.

In the second column of Fig. 3, the foreground object in the input image appears to be illuminated from the right, whereas the background is a cloudy image. Ideally, under such background illumination, the foreground object should have smooth lighting. The result of Lalonde et al. [21] is in-

	fMAE↓	fPSNR↑	fSSIM↑	LPIPS↓
HDR Illum. map	0.097	19.91	0.858	0.017
Ours	0.066	22.75	0.899	0.011

Table 3. Quantitative comparison of HDR illumination maps for image harmonization on the test set.

	fMAE↓	fPSNR↑	fSSIM↑
Baseline NRF	0.057	22.77	0.874
Baseline NRF + F_a	0.054	23.64	0.908
Baseline NRF + F_a + \hat{I}	0.051	24.43	0.916
Baseline NRF + F_a + \hat{I} + SSIM loss	0.049	24.66	0.938

Table 4. Ablation study on neural rendering framework.

consistent in terms of both color and illumination. Although Rainnet [22], Dovenet [10] and Guo et al. [16] produce results that are a step closer to the ground truth, the highlights at the man’s left shoulder are improperly preserved. Our method not only effectively delights the foreground object, but also re-renders it under smooth illumination.

5.3. Comparison with HDR illumination map

The efficacy of our learned illumination descriptor is compared with the HDR illumination representation within our framework. Specifically, we learn an encoder-decoder based neural network to map the given background image to its corresponding panoramic HDR illumination map. We train this network until its loss converges. Then, we use it to estimate the HDR panoramic image from the background image. The estimated HDR image is further used as part of our neural rendering framework. The rendered images are compared against those generated using our learned illumination descriptor, which is reported in Tab. 3. Note that our learned illumination descriptors achieve significantly better performance compared to the estimated HDR images.

5.4. Ablation Study

The ablation studies are conducted to demonstrate the effectiveness of each component on the neural rendering framework.

Neural rendering framework Ablation. We demonstrate how the use of the albedo features F_a and the input unharmonized image \hat{I} as additional inputs to the Rendering Module can improve its performance. We also perform an ablation on the loss function of our neural rendering framework. Results of this ablation study are reported in Tab. 4.

We start with the Baseline NRF which uses the concatenated shading and albedo images as inputs to the Rendering Module. Replacing the albedo image with the albedo feature F_a results in better performances. This is mainly because the albedo feature F_a contains richer information.

We then proceed to add the input unharmonized image

K	4	8	16	32	64
fPSNR↑	31.85	32.50	32.81	32.82	32.84
fSSIM↑	0.960	0.962	0.966	0.966	0.967

Table 5. Effects of the number K of shading bases.

\hat{I} in conjunction with the albedo feature F_a and the shading image as inputs to the Rendering Module, and observe noticeable improvements in performance. The delighting, which occurs as a consequence of albedo estimation, can result in a loss of information in the final rendered image. Therefore, using the unharmonized image \hat{I} as additional input can make up for the lost information.

Finally, in addition to the \mathcal{L}_1 loss of the baseline NRF, the SSIM loss function is added. Experimental results show adding the SSIM loss significantly improves the performance of our framework, especially in terms of the foreground SSIM (fSSIM) metric measurement.

Effects of the number K of shading bases. To measure the influence of the number K of shading bases on the performance of our Shading Module, we train the Shading Module with 5 different values of K (4, 8, 16, 32, 64). Tab. 5 reports the results under different settings. Note that the reported metrics (fPSNR, fSSIM) are obtained by comparing the results generated by our Shading Module against the corresponding ground truth shading images. There exists a significant increase in the performance when the value of K increases from 4 to 16, then the increase becomes less obvious when $K > 16$. To balance between rendering performance and computational complexity, we resolve to use $K = 32$ as the optimal number of shading bases.

6. Conclusion

In this paper, we have contributed a large-scale photo-realistic image harmonization dataset. In addition, a novel neural rendering framework is designed to learn a direction-aware illumination descriptor from the illumination maps. A neural shading module is proposed to generate the foreground shading using the direction-aware illumination descriptor estimated from the background. Extensive experiments on our constructed dataset demonstrate the effectiveness of our proposed method.

Limitations. This work also has a few limitations that can be the subject of future work. 1) We only focus on a specific object type (human body), which limits the application scope of our method. Extending to more types of objects could improve the ability to generalize across a wide spectrum of objects. 2) Only Lambertian objects are considered. When introducing the specular BRDFs [4], our model could be applied to the objects with specular reflection.

References

- [1] 3D People. <https://3dpeople.com>. 3
- [2] HDR MAPS. <https://hdrmaps.com/>. 3
- [3] Poly Haven. <https://polyhaven.com/hdris>. 3
- [4] Michael Ashikmin, Simon Premože, and Peter Shirley. A microfacet-based brdf generator. In *Proceedings of the 27th annual conference on Computer graphics and interactive techniques*, pages 65–74, 2000. 8
- [5] Peter N Belhumeur and David J Kriegman. What is the set of images of an object under all possible illumination conditions? *International journal of computer vision*, 28(3):245–260, 1998. 4
- [6] Daniel Cohen-Or, Olga Sorkine, Ran Gal, Tommer Leyvand, and Ying-Qing Xu. Color harmonization. In *ACM SIGGRAPH 2006 Papers*, pages 624–630. 2006. 2
- [7] Blender Online Community. *Blender - a 3D modelling and rendering package*. Blender Foundation, Stichting Blender Foundation, Amsterdam, 2018. 3
- [8] Wenyan Cong, Junyan Cao, Li Niu, Jianfu Zhang, Xuesong Gao, Zhiwei Tang, and Liqing Zhang. Deep image harmonization by bridging the reality gap, 2021. 1, 2
- [9] Wenyan Cong, Li Niu, Jianfu Zhang, Jing Liang, and Liqing Zhang. Bargainnet: Background-guided domain translation for image harmonization. In *2021 IEEE International Conference on Multimedia and Expo (ICME)*, pages 1–6. IEEE, 2021. 2
- [10] Wenyan Cong, Jianfu Zhang, Li Niu, Liu Liu, Zhixin Ling, Weiyuan Li, and Liqing Zhang. Dovenet: Deep image harmonization via domain verification. In *CVPR*, 2020. 1, 2, 6, 7, 8
- [11] Xiaodong Cun and Chi-Man Pun. Improving the harmony of the composite image by spatial-separated attention module. *IEEE Transactions on Image Processing*, 29:4759–4771, 2020. 2
- [12] Paul Debevec. Image-based lighting. In *ACM SIGGRAPH 2006 Courses*, pages 4–es. 2006. 1
- [13] Paul Debevec, Tim Hawkins, Chris Tchou, Haarm-Pieter Duiker, Westley Sarokin, and Mark Sagar. Acquiring the reflectance field of a human face. In *Proceedings of the 27th annual conference on Computer graphics and interactive techniques*, pages 145–156, 2000. 2
- [14] Paul E. Debevec and Jitendra Malik. Recovering high dynamic range radiance maps from photographs. In *Proceedings of the 24th Annual Conference on Computer Graphics and Interactive Techniques*, SIGGRAPH '97, page 369–378, USA, 1997. ACM Press/Addison-Wesley Publishing Co. 1
- [15] Ulrich Fecker, Marcus Barkowsky, and André Kaup. Histogram-based prefiltering for luminance and chrominance compensation of multiview video. *IEEE Transactions on Circuits and Systems for Video Technology*, 18(9):1258–1267, 2008. 1
- [16] Zonghui Guo, Haiyong Zheng, Yufeng Jiang, Zhaorui Gu, and Bing Zheng. Intrinsic image harmonization. In *Proceedings of the IEEE/CVF Conference on Computer Vision and Pattern Recognition (CVPR)*, pages 16367–16376, June 2021. 1, 2, 6, 7, 8
- [17] Guoqing Hao, Satoshi Iizuka, and Kazuhiro Fukui. Image harmonization with attention-based deep feature modulation. In *BMVC*, 2020. 2
- [18] Jiaya Jia, Jian Sun, Chi-Keung Tang, and Heung-Yeung Shum. Drag-and-drop pasting. *ACM Transactions on Graphics (SIGGRAPH)*, 2006. 2
- [19] Yoshihiro Kanamori and Yuki Endo. Relighting humans: occlusion-aware inverse rendering for full-body human images. *ACM Transactions on Graphics (TOG)*, 37(6):1–11, 2018. 2
- [20] Manuel Lagunas, Xin Sun, Jimei Yang, Ruben Villegas, Jianming Zhang, Zhixin Shu, Belen Masia, and Diego Gutierrez. Single-image full-body human relighting. *arXiv preprint arXiv:2107.07259*, 2021. 2
- [21] Jean-Francois Lalonde and Alexei A Efros. Using color compatibility for assessing image realism. In *2007 IEEE 11th International Conference on Computer Vision*, pages 1–8. IEEE, 2007. 1, 2, 6, 7
- [22] Jun Ling, Han Xue, Li Song, Rong Xie, and Xiao Gu. Region-aware adaptive instance normalization for image harmonization. In *Proceedings of the IEEE/CVF Conference on Computer Vision and Pattern Recognition*, pages 9361–9370, 2021. 1, 2, 6, 7, 8
- [23] Abhimitra Meka, Christian Haene, Rohit Pandey, Michael Zollhöfer, Sean Fanello, Graham Fyffe, Adarsh Kowdle, Xueming Yu, Jay Busch, Jason Dourgarian, et al. Deep reflectance fields: high-quality facial reflectance field inference from color gradient illumination. *ACM Transactions on Graphics (TOG)*, 38(4):1–12, 2019. 2
- [24] Mark Pauly, Richard Keiser, Leif P Kobbelt, and Markus Gross. Shape modeling with point-sampled geometry. *ACM Transactions on Graphics (TOG)*, 22(3):641–650, 2003. 4
- [25] Patrick Pérez, Michel Gangnet, and Andrew Blake. Poisson image editing. In *ACM SIGGRAPH 2003 Papers*, pages 313–318. 2003. 2
- [26] Francois Pitie, Anil C Kokaram, and Rozenn Dahyot. N-dimensional probability density function transfer and its application to color transfer. In *Tenth IEEE International Conference on Computer Vision (ICCV'05) Volume 1*, volume 2, pages 1434–1439. IEEE, 2005. 2
- [27] François Pitié, Anil C Kokaram, and Rozenn Dahyot. Automated colour grading using colour distribution transfer. *Computer Vision and Image Understanding*, 107(1-2):123–137, 2007. 1, 2
- [28] Ravi Ramamoorthi and Pat Hanrahan. An efficient representation for irradiance environment maps. In *Proceedings of the 28th annual conference on Computer graphics and interactive techniques*, pages 497–500, 2001. 1, 2
- [29] Erik Reinhard, Michael Adhikhmin, Bruce Gooch, and Peter Shirley. Color transfer between images. *IEEE Computer graphics and applications*, 21(5):34–41, 2001. 1, 2
- [30] Olaf Ronneberger, Philipp Fischer, and Thomas Brox. U-net: Convolutional networks for biomedical image segmentation. In *International Conference on Medical image computing and computer-assisted intervention*, pages 234–241. Springer, 2015. 4

- [31] Shen Sang and Manmohan Chandraker. Single-shot neural relighting and svbrdf estimation. In *European Conference on Computer Vision*, pages 85–101. Springer, 2020. 2
- [32] Konstantin Sofiiuk, Polina Popenova, and Anton Konushin. Foreground-aware semantic representations for image harmonization. In *Proceedings of the IEEE/CVF Winter Conference on Applications of Computer Vision*, pages 1620–1629, 2021. 2
- [33] Shuangbing Song, Fan Zhong, Xueying Qin, and Changhe Tu. Illumination harmonization with gray mean scale. In *Computer Graphics International Conference*, pages 193–205. Springer, 2020. 2
- [34] Tiancheng Sun, Jonathan T Barron, Yun-Ta Tsai, Zexiang Xu, Xueming Yu, Graham Fyffe, Christoph Rhemann, Jay Busch, Paul E Debevec, and Ravi Ramamoorthi. Single image portrait relighting. *ACM Trans. Graph.*, 38(4):79–1, 2019. 2
- [35] Kalyan Sunkavalli, Micah K Johnson, Wojciech Matusik, and Hanspeter Pfister. Multi-scale image harmonization. *ACM Transactions on Graphics (TOG)*, 29(4):1–10, 2010. 2
- [36] Yi-Hsuan Tsai, Xiaohui Shen, Zhe Lin, Kalyan Sunkavalli, Xin Lu, and Ming-Hsuan Yang. Deep image harmonization. In *Proceedings of the IEEE Conference on Computer Vision and Pattern Recognition*, pages 3789–3797, 2017. 1, 2, 4
- [37] Zhou Wang, Alan C Bovik, Hamid R Sheikh, and Eero P Simoncelli. Image quality assessment: from error visibility to structural similarity. *IEEE transactions on image processing*, 13(4):600–612, 2004. 6
- [38] Zhibo Wang, Xin Yu, Ming Lu, Quan Wang, Chen Qian, and Feng Xu. Single image portrait relighting via explicit multiple reflectance channel modeling. *ACM Transactions on Graphics (TOG)*, 39(6):1–13, 2020. 2
- [39] Xuezhong Xiao and Lizhuang Ma. Color transfer in correlated color space. In *Proceedings of the 2006 ACM international conference on Virtual reality continuum and its applications*, pages 305–309, 2006. 1
- [40] Zexiang Xu, Kalyan Sunkavalli, Sunil Hadap, and Ravi Ramamoorthi. Deep image-based relighting from optimal sparse samples. *ACM Transactions on Graphics (TOG)*, 37(4):1–13, 2018. 2
- [41] Su Xue, Aseem Agarwala, Julie Dorsey, and Holly Rushmeier. Understanding and improving the realism of image composites. *ACM Transactions on graphics (TOG)*, 31(4):1–10, 2012. 1, 2
- [42] Ye Yu, Abhimitra Meka, Mohamed Elgharib, Hans-Peter Seidel, Christian Theobalt, and William AP Smith. Self-supervised outdoor scene relighting. In *European Conference on Computer Vision*, pages 84–101. Springer, 2020. 2
- [43] Richard Zhang, Phillip Isola, Alexei A Efros, Eli Shechtman, and Oliver Wang. The unreasonable effectiveness of deep features as a perceptual metric. In *CVPR*, 2018. 6
- [44] Yulun Zhang, Yapeng Tian, Yu Kong, Bineng Zhong, and Yun Fu. Residual dense network for image super-resolution. In *Proceedings of the IEEE conference on computer vision and pattern recognition*, pages 2472–2481, 2018. 4
- [45] Hang Zhao, Orazio Gallo, Iuri Frosio, and Jan Kautz. Loss functions for image restoration with neural networks. *IEEE Transactions on computational imaging*, 3(1):47–57, 2016. 6
- [46] Hao Zhou, Sunil Hadap, Kalyan Sunkavalli, and David W Jacobs. Deep single-image portrait relighting. In *Proceedings of the IEEE International Conference on Computer Vision*, pages 7194–7202, 2019. 2
- [47] Jun-Yan Zhu, Philipp Krahenbuhl, Eli Shechtman, and Alexei A Efros. Learning a discriminative model for the perception of realism in composite images. In *Proceedings of the IEEE International Conference on Computer Vision*, pages 3943–3951, 2015. 1, 2